Title	Charge-changing cross sections of fast H-0,H-1+ and He-0,He-1+,He-2+ projectiles in C-60
Author(s)	Itoh, A; Nose, K; Hamamoto, Y; Mizuno, T; Ishii, K
Citation	PHYSICAL REVIEW A (2005), 72(5)
Issue Date	2005-11-23
URL	http://hdl.handle.net/2433/52651
Right	Copyright 2005 American Physical Society
Type	Journal Article
Textversion	publisher; none

Charge-changing cross sections of fast $H^{0,1+}$ and $He^{0,1+,2+}$ projectiles in C_{60}

A. Itoh,[1] K. Nose,[1] Y. Hamamoto,[1] T. Mizuno,[1] and K. Ishii[2]
[1]*Quantum Science and Engineering Center, Kyoto University, Kyoto 606-8501, Japan*
[2]*Department of Physics, Nara Women's University, Nara 630-8506, Japan*
(Received 23 August 2005; published 23 November 2005)

Electron capture and loss cross sections have been measured for fast light projectile ions of 0.5 MeV $H^{0,1+}$ and 0.5–2.0 MeV $^4He^{0,1+,2+}$ in collisions with C_{60}. The gaseous target of C_{60} was prepared by heating C_{60} powder in a target cell to temperatures of 300–500 °C, and outgoing charge fractions were measured as a function of the cell temperature. Absolute cross sections are deduced by using two different vapor-pressure data available in literature. Experimental cross sections are examined in comparison with theoretical values obtained from various conventional formulas proposed for atomic targets. In addition, single- and double-electron capture cross sections are also calculated on the basis of a classical model by taking account of the local electron density of C_{60}. From a complete set of our experimental cross sections, equilibrium charge fractions are also deduced and found to be essentially the same as carbon-foil data, indicating no gas-solid difference.

DOI: 10.1103/PhysRevA.72.052718 PACS number(s): 34.70.+e

I. INTRODUCTION

Since the epochmaking discovery of C_{60} in 1985 [1], fullerene molecules have attracted considerable attention in atomic collision physics as a promising collision partner providing new information about the nature of matter lying between atoms and solids. Much effort has been devoted so far to study of a variety of collision-induced phenomena involving fullerene molecules such as fragmentation and ionization of free molecules or fusion reactions between two fullerenes by using either gas-phase targets or accelerated fullerene beams (see, e.g., Ref. [2], and references therein). On the contrary, much less is known, for various inelastic collisions, about their absolute values of cross sections which are indispensable to achieve accurate and quantitative understanding of collision processes.

For instance, the charge-changing collision, in which a projectile particle changes its charge state via electron capture and loss collisions during passing through a target medium, is one of the most fundamental inelastic processes. Nevertheless, absolute charge-changing cross sections have been measured only for slow ions [3–6] and no data are available for energetic fast projectile ions. From a theoretical aspect, electron capture by a slow ion with a velocity much smaller than the Bohr velocity ($v_0=2.2\times10^8$ cm/s) can be described satisfactorily by a classical overbarrier (COB) model [7,8]. At high velocities, on the other hand, no theoretical model has been proposed so far concerning polyatomic molecules like C_{60}. It is known in radiation physics that the energy loss of swift charged particles in molecules can be approximated by the sum of individual energy loss for constituent atoms in the molecule [9]. This additive rule is also known to hold for charge-changing collisions of fast hydrogen projectiles with gaseous hydrocarbon targets [10]. The validity of this additive rule is, however, an open question to what extent the rule holds and, in the present case, whether it is possible to obtain charge-changing cross sections for C_{60} from atomic carbon cross sections which may be calculated by using available theoretical formulas.

In this work we investigate the charge-changing process of fast light projectiles passing through a C_{60} gas target and present absolute cross sections for electron capture and loss collisions. It is noted that experimental data of the C_{60} vapor pressure show a large spread in the literature with discrepancies of about one order of magnitude [11–14]. Therefore, we present here two sets of cross section data deduced from two different vapor pressure data. One is taken from [11] which is recognized as containing the most reliable values as examined in [5,6], and the other is taken from [14] which has been reported more recently.

This paper is organized as follows. The experimental arrangement and the procedure to determine cross sections are described in Sec. II. Theoretical formulas for electron capture and loss cross sections used in this work are described in detail in Sec. III. Experimental cross sections are presented in Sec. IV and examined in comparison with theoretical values. A discussion is also given in Sec. IV about equilibrium charge fractions deduced from the present cross sections.

II. EXPERIMENTAL METHOD

The experiment was performed at the QSEC heavy-ion accelerator facility of Kyoto University. Projectile particles were $^4He^{0,1+,2+}$ at incident energies of 0.5, 1.0, 1.5, and 2.0 MeV and 0.5 MeV $H^{0,1+}$. An outline of the experiment is described below for helium projectiles. A beam of He^{q+} ($q=1,2$) ions extracted from a Van de Graaff accelerator was carefully collimated with a two-dimensional jaw slit to smaller than 0.2 mm in diameter. The beam was then charge purified with a magnetic charge selector before entering a C_{60} gas cell as sketched in Fig. 1. The outgoing beam with various charge states was magnetically charge separated and detected by solid-state detectors (SSD's). As for He^0 incidence, neutral particles produced in the beamline via collisions of a primary He^+ beam with residual gases were used by removing all the charged particles by a magnet before the collision cell. The background pressure was about 5×10^{-7} Torr during the course of measurements.

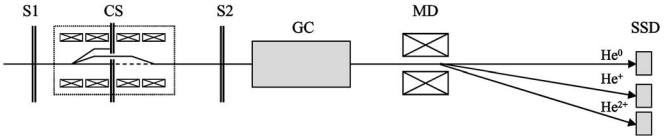

FIG. 1. A schematic diagram of experimental apparatus. S1, S2: two-dimensional collimator slits. CS: magnetic charge selector. GC: gas cell of C_{60}. MD: magnetic charge deflector. SSD: solid-state detector.

The target gas cell was an 80-mm-long stainless-steel cylinder with an outer diameter 33 mm and is equipped with a built-in resistive heater. The net size of the gas target is 50 mm long and 8 mm in diameter. Entrance and exit apertures of the cell are 1 mm and 1.5 mm in diameter, respectively. The cell contains C_{60} powder of purity 99.98% and can be resistively heated up to temperatures of 500 °C at maximum. The cell temperature was measured by an ac thermocouple connected to the inner surface of the cell and was stabilized within ±1 °C. Before experiments the C_{60} powder was preheated at the maximum temperature of 500 °C for several hours to remove any contaminating solvents.

Charge fraction measurements were performed at cell temperatures ranging from 300 to 500 °C. The C_{60} gas pressure P (Torr) at a temperature T (K) inside the cell was calculated by using two vapor pressure data reported by Abrefah *et al.* [11] and by Jaeansch and Kamke [14] expressed, respectively, as follows:

$$P_{(\mathrm{ab})} = 10^{7.592-8309/T}, \tag{1}$$

$$P_{(\mathrm{ja})} = 10^{8.895-8801/T}. \tag{2}$$

Note that ratios $P_{(\mathrm{ja})}/P_{(\mathrm{ab})}$ are 2.78 at 300 °C and 4.64 at 500 °C. The number density N_t (molecules/cm^3) of C_{60} was determined by applying the ideal gas law as

$$N_t = 2.69 \times 10^{19} \frac{P}{760} \frac{273}{T}. \tag{3}$$

The target thickness is defined by N_t times the effective length of the gas cell. We evaluated the effective length by calculating the C_{60} number density along the beamline due to a gas flow out of the cell. It turned out that the effective length was increased by about 15% at 500 °C compared to the geometrical cell length of 50 mm.

The charge fraction f_q in the outgoing beam is obtained by $I_q/\Sigma_k I_k$ in terms of the number of particles I_k of charge state k detected by SSD's. The rate equation of $f_q(x)$ as a function of the target thickness is written as

$$\frac{d}{dx}\begin{pmatrix} f_0 \\ f_1 \\ f_2 \end{pmatrix} = \begin{pmatrix} -\sigma_{00} & \sigma_{10} & \sigma_{20} \\ \sigma_{01} & -\sigma_{11} & \sigma_{21} \\ \sigma_{02} & \sigma_{12} & -\sigma_{22} \end{pmatrix} \begin{pmatrix} f_0 \\ f_1 \\ f_2 \end{pmatrix} \tag{4}$$

or, equivalently, as

$$\frac{d}{dx}\boldsymbol{f} = S\boldsymbol{f}, \tag{5}$$

where σ_{qk} stands for the charge changing cross section from charge state q to k and $\sigma_{qq} \equiv \Sigma_{k\neq q}\sigma_{qk}$. In a low-pressure region where a single collision condition holds, the fraction f_k feeding from an initial charge q may be approximated by

$$f_k(x) = f_k(0) + \sigma_{qk}x. \tag{6}$$

The cross section σ_{qk} can, therefore, be obtained from this formula by subtracting $f_k(0)$, the initial fraction at the background gas pressure.

We used, instead, a comprehensive way to obtain more accurate cross sections as follows. The rate equation given above is an elementary eigenvalue problem and can be solved analytically once all the matrix elements of S are known. Namely, the solution is expressed in a form of

$$\boldsymbol{f}(x) = \sum_{i=1}^{3} c_i \boldsymbol{u}_i e^{\lambda_i x}, \tag{7}$$

by using eigenvalues λ_i and eignevectors $\boldsymbol{u}_i$ of the matrix S, and c_i is the constant value determined from the initial charge fractions. Note $\lambda_3 = 0$. As for hydrogen projectiles, the fractions are obtained straightforwardly. In the case of H^0 incidence, two fractions are written by

$$f_1(x) = \frac{\sigma_{01}}{\sigma_{01}+\sigma_{10}}(1 - e^{-(\sigma_{01}+\sigma_{10})x}),$$

$$f_0(x) = 1 - f_1(x).$$

Equation (7) was fitted to the experimental fraction curves for all the incident charge states, and a complete set of cross sections was deduced by iterative calculations starting with initial cross sections estimated by Eq. (6). The overall uncertainties of the present cross sections arising from errors of counting statistic and target thickness are about 10%, but the largest systematic ambiguity comes from the choice of the vapor pressure data [11,14].

Furthermore, Eq. (7) gives equilibrium charge fractions attained at $x \to \infty$, for which the fractions are given by the third term as

$$\boldsymbol{f}(\infty) = c_3 \boldsymbol{u}_3 \tag{8}$$

because the eigenvalues λ_1 and λ_2 are negative. As for hydrogen projectiles,

$$f_0(\infty) = \frac{\sigma_{01}}{\sigma_{01}+\sigma_{10}}, \quad f_1(\infty) = 1 - f_0(\infty).$$

The equilibrium fractions estimated in this way are also discussed below.

III. THEORETICAL CALCULATION

The charge-changing collision has been a long-term subject in the last century and several review articles [15–18] as well as some textbooks [19,20] are available. Nevertheless, quantum mechanical calculations of electron capture and loss

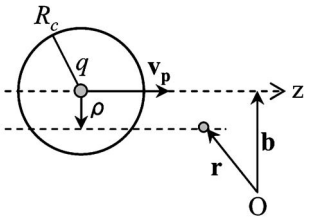

FIG. 2. A schematic view of collision between an ion with charge q and a C_{60} centered at O. z is the direction of the ion with a velocity v_p, $\boldsymbol{b}$ the impact parameter of the ion with respect to the C_{60} center. $\boldsymbol{r}$ is the position vector of an target electron with impact parameter $\boldsymbol{\rho}$ with respect to the incident ion.

cross sections are limited to rather simple collision systems relevant mostly to atomic targets. In this sense, the classical picture pioneered by Bohr [21,22] gives still at present a useful estimation of the magnitude of cross sections for molecular targets. In this section, Bohr's classical formulas and their extension to C_{60} are described briefly.

In Ref. [21] Bohr derived capture and loss cross sections for collisions between light projectiles and intermediate atomic targets, as follows:

$$\sigma_{q,q-1} = 4\pi a_0^2 q^2 z_1^3 z_2^{1/3} \left(\frac{v_0}{v_p}\right)^6 \tag{9}$$

for single-electron capture and

$$\sigma_{z_1-1,z_1} = \pi a_0^2 z_1^{-1} z_2^{2/3} \left(\frac{v_0}{v_p}\right) \tag{10}$$

for single-electron loss from a hydrogen-like ion, where v_p is the ion velocity, z_1 and z_2 are atomic numbers of the two particles, and $a_0 = 0.529 \times 10^{-8}$ cm is the Bohr radius. Corresponding cross sections for C_{60} may be obtained from these formulas by multiplying by 60, the number of constituent carbon atoms.

We also calculated capture cross sections for C_{60} in a more realistic way as follows. As an extension of the electron capture model of Bohr and Lindhard [22], Brandt [23] and later on Ben-Itzhak *et al.* [24] derived a formulation to calculate impact-parameter-dependent capture probability in ion-H collisions. According to the method of Ben-Itzhak *et al.*, the single-electron capture probability $p(b)$ at an impact parameter b is obtained by

$$p(b) = \int \frac{2}{v_p} \sqrt{R_c^2 - \rho^2} \frac{1}{\tau(\boldsymbol{r})} n_1(\boldsymbol{r}) d^3\boldsymbol{r}, \tag{11}$$

where the first term $(2\sqrt{R_c^2 - b^2}/v_p)$ represents the duration of a target electron staying inside the capture radius defined as $R_c \simeq 2q/v_p^2$. The second term $1/\tau(\boldsymbol{r})$ is the release rate of the target electron per second and is obtained from the uncertainty principle $\tau(\boldsymbol{r}) E_e(\boldsymbol{r}) \sim \hbar$, with $E_e(\boldsymbol{r})$ the local electron energy. The third term $n_1(\boldsymbol{r})$ is the local electron density of a hydrogen atom.

We applied the above formula to C_{60} molecule as follows. Figure 2 depicts a collision scheme in our calculations, and atomic units are used hereafter. Puska and Nieminen [25] calculated the local electron density $n(\boldsymbol{r})$ of C_{60} using a jellium model, which may be approximated to a good accuracy by the following analytical formula [26]:

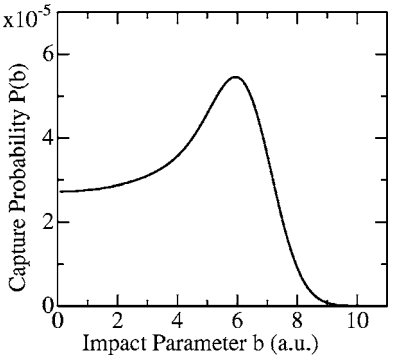

FIG. 3. Single-electron capture probability $p(b)$ as a function of the impact parameter b calculated for 2 MeV He^{2+} incidence.

$$n(\boldsymbol{r}) = 0.146 e^{-(r-6.6)^2/2.7} = 240 n_1(\boldsymbol{r}), \tag{12}$$

with

$$\int n_1(\boldsymbol{r}) d^3\boldsymbol{r} = 1.$$

As for $\tau(\boldsymbol{r})$, we used the relationship $1/\tau(\boldsymbol{r}) = E_e(\boldsymbol{r}) = v_e^2(\boldsymbol{r})/2$, with the local Fermi velocity $v_e = [3\pi^2 n(\boldsymbol{r})]^{1/3}$. The probability of one-electron capture from C_{60} is therefore calculated by

$$p(b) = (720\pi^2)^{2/3} \frac{R_c}{v_p} \int_0^{R_c} \int_0^{2\pi} \int_{-\infty}^{\infty} \sqrt{1 - \frac{\rho^2}{R_c^2}} n_1(r)^{5/3} \rho d\rho d\phi dz, \tag{13}$$

with the relationship $r^2 = b^2 + \rho^2 + z^2 + 2b\rho\cos\phi$, where ϕ is the angle between $\boldsymbol{b}$ and $\boldsymbol{\rho}$ in cylindrical coordinates (not shown explicitly in Fig. 2). Figure 3 shows an example of the impact-parameter-dependent capture probability calculated for 2 MeV He^{2+} incidence.

Finally, the cross section for the capture of i electrons from N (=240) electrons is obtained by employing the independent-electron model as

$$\sigma_i = {}_N C_i 2\pi \int_0^{\infty} p^i(b)[1 - p(b)]^{N-i} b db. \tag{14}$$

IV. RESULTS AND DISCUSSION

A. Cross sections and equilibrium charge fractions

Figure 4 shows background-subtracted growth curves of charge fractions measured for 1 MeV $He^{0,1+,2+}$ incidences. The abscissa x is the C_{60} thickness obtained from the vapor pressure $P_{(ab)}$ [11]. Solid curves are calculated results, according to Eq. (7), determined by iterative fitting calculations starting with initial cross sections obtained from Eq. (6) at low gas pressures. Obviously, our fitting calculations can reproduce almost perfectly all the experimental growth curves.

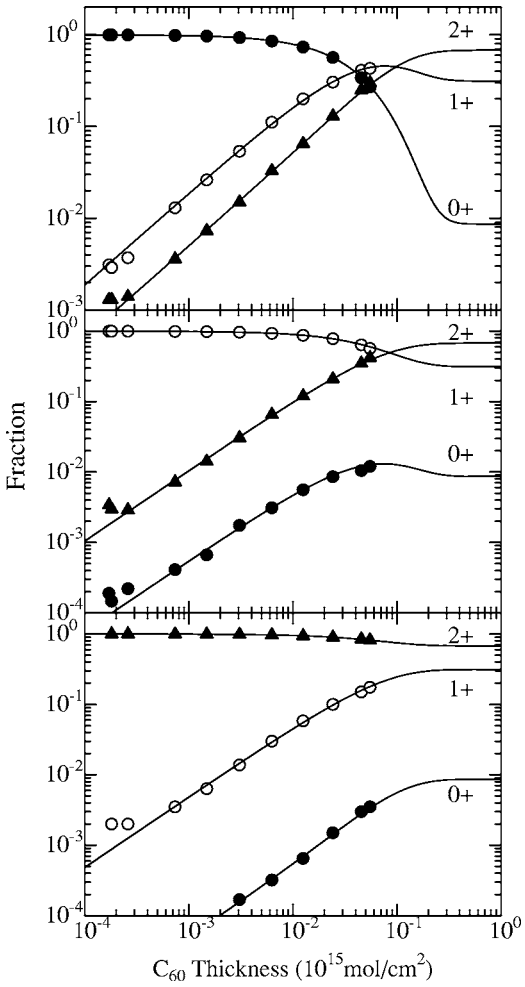

FIG. 4. Charge fractions $f_k(x)$ $(k=0-2)$ measured for 1 MeV He^{q+} $(q=0-2)$ incident beams. Data are plotted as a function of the C_{60} gaseous target thickness x determined from the pressure data in [11].

It turned out that the final cross sections do not differ much from the initial values, being coincident with each other within several percent at most. It is noted that all the arguments given above hold exactly the same for the case of the vapor pressure of $P_{(ja)}$ [14].

Capture and loss cross sections obtained in this way are listed in Table I, where two sets of data are given corresponding to two different vapor pressure data [11,14]. Ratios between these two cross sections are about 4.4 on average. It is interesting to point out that the cross sections are surprisingly large, and some of them exceed greatly the geometrical cross section, 38×10^{-16} cm^2, of C_{60}. When we compare these cross sections with those obtained for other gaseous targets of, e.g., N_2, they are roughly from 10 (P_{ja}) to 50 (P_{ab}) times larger than corresponding N_2 cross sections [27–29]. It is interesting to note that the difference is equivalent to the ratio of 30 between the number of constituent atoms in C_{60} and N_2, indicating $\sigma(C)\simeq\sigma(N)$.

As can be seen in Fig. 4, the calculated growth curves depict also equilibrium charge fractions at higher target thicknesses. Experimentally we could not obtain these equilibrated values due to the limit of maximum temperature of our gas cell. The equilibrium fractions, as expressed by Eq. (8), are constant values independent of both x and the incident charge state. Such equilibration fractions are found, in the case of $P_{(ab)}$, to be attained at thicknesses over some 10^{14} mol/cm^2 for both H and He incidences. Putting this target thickness at 5×10^{14} mol/cm^2 and assuming 3×10^{-14} cm^2 as a total charge-changing cross section, the "mean free path" is estimated to be about 3.3 mm. It implies that the charge equilibration is attained after about 15 times charge-changing collisions in our 5-cm-long gas cell. This estimation is reasonably consistent with previous experimental data for gaseous targets as reviewed by Betz [15].

The estimated equilibrium fractions are listed in Table II. Obviously there is no essential difference between two data deduced from $P_{(ab)}$ and $P_{(ab)}$. As depicted in Fig. 5, the equilibrium fractions are found to compare fairly well with carbon-foil data (solid lines) [30], indicating no gas-solid difference for gaseous C_{60} and solid carbon foils. This result may be attributed to a fact that, in the present low-z_1 projectiles, only the $1s$ state is involved predominantly in capture and loss collisions. This is because electron capture into excited states, which is commonplace in highly charged slow collisions [31,32], may be negligibly small in the present velocity region.

TABLE I. Electron capture and loss cross sections (10^{-16} cm^2) in collisions of $He^{0,1+,2+}$ and $H^{0,1+}$ with C_{60}. The upper values are deduced from the vapor pressure data in [11], and the lower ones in parentheses are from [14].

	He^{q+}						H^{q+}	
E (MeV)	σ_{01}	σ_{02}	σ_{12}	σ_{10}	σ_{21}	σ_{20}	σ_{01}	σ_{10}
0.5	261	59.7	76.6	20.1	100	9.48	149	0.452
	(62.0)	(14.1)	(17.7)	(4.62)	(22.6)	(2.13)	(34.1)	(0.104)
1.0	187	51.3	105	5.50	48.6	0.494		
	(44.0)	(11.5)	(23.9)	(1.18)	(9.66)	(0.11)		
1.5	182	73.5	98.0	1.97	9.93	0.0888		
	(41.2)	(16.1)	(22.2)	(0.438)	(2.19)	(0.0195)		
2.0	169	60.1	94.4	0.597	4.96	0.0263		
	(37.9)	(13.3)	(23.1)	(0.134)	(1.10)	(0.00578)		

TABLE II. Equilibrium charge fractions and mean charges of helium and hydrogen projectiles passing through a C_{60} gas target obtained from the cross sections in Table I. The upper and lower values correspond to [11,14], respectively.

	He				H		
E (MeV)	F_0	F_1	F_2	$\langle q \rangle$	F_0	F_1	$\langle q \rangle$
0.5	4.63	54.6	40.8	1.36	0.302	99.7	0.997
	(4.45)	(54.2)	(41.34)	(1.37)	(0.304)	(99.7)	(0.997)
1.0	0.863	31.3	67.84	1.67			
	(0.747)	(28.6)	(70.7)	(1.70)			
1.5	0.102	9.19	90.7	1.91			
	(0.0996)	(8.977)	(90.9)	(1.91)			
2.0	0.0239	5.00	95.0	1.95			
	(0.0227)	(4.56)	(95.4)	(1.95)			

B. Comparison with theory

Electron capture cross sections for helium projectiles are plotted in Fig. 6 together with theoretical calculations. Here we show two sets of experimental data given in Table I. Dashed lines are single-electron capture cross sections calculated by Bohr's formula, Eq. (9). Obviously this formula gives fairly comparable values with experimental values. Thus, it can certainly be stated that a cross section for a molecule can be obtained from an atomic cross section multiplied by the number of atoms in the molecule; i.e., the additive rule holds also for fast helium projectiles as was observed for fast hydrogen projectiles in various hydrocarbon molecules [10].

On the other hand, more elaborate calculations of Eqs. (13) and (14) (solid lines), taking account of the spatial electron distribution, give rather small cross sections of σ_{10} and σ_{21} compared to experimental values. As for double-capture cross sections σ_{20}, however, calculated results are fortuitously in good agreement with experiments, although the dependence on the impact energy is somewhat different. One possible reason for the discrepancy of single-capture cross sections may be attributed to our incorrect use of the electron release rate $1/\tau(\boldsymbol{r})=E_e(\boldsymbol{r})$ in Eq. (11). In the original model of Bohr and Lindhard [22], the release rate is defined as the order of v_e/(electron orbital radius). If we use this relationship as $1/\tau(\boldsymbol{r})=v_e(\boldsymbol{r})/a_0$, capture cross sections are found to increase to a factor of 1.5 larger values compared with the solid lines in the figure and they become overlapping with experimental data. Another possible reason is that, in the preset model, only valence electrons of C_{60} are taken into consideration and capture from carbon $1s$ electrons is not included. As our projectile velocities are rather fast, the $1s$-$1s$ electron transfer seems contribute noticeably. This K-K transfer was also calculated by using formulas given in [33] for σ_{10} and σ_{21} by multiplying by 60. Results are shown

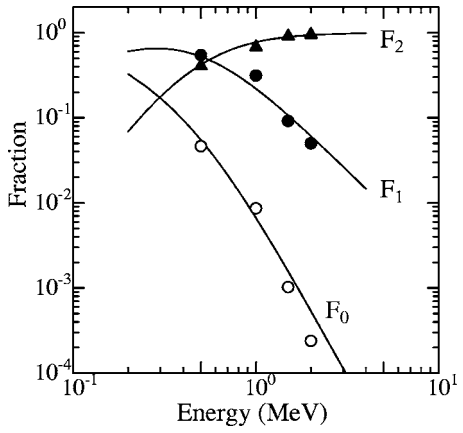

FIG. 5. Equilibrium charge fractions deduced from the present cross sections. Solid lines are carbon foil data [30].

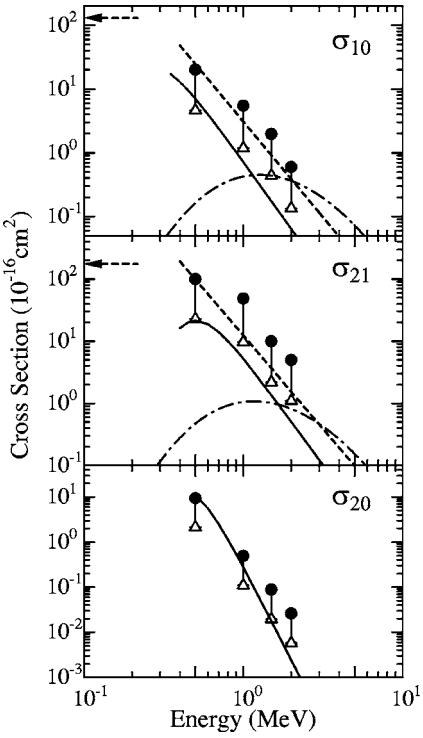

FIG. 6. Electron capture cross sections for helium projectiles. Solid circles and open triangles correspond to the vapor pressure data of [11,14], respectively. Theoretical values: dashed lines from Eq. (9), solid lines from Eq. (14), dot-dashed lines representing $1s$-$1s$ transfer cross sections from [33]. Dashed arrows depict values of the COB model (see text).

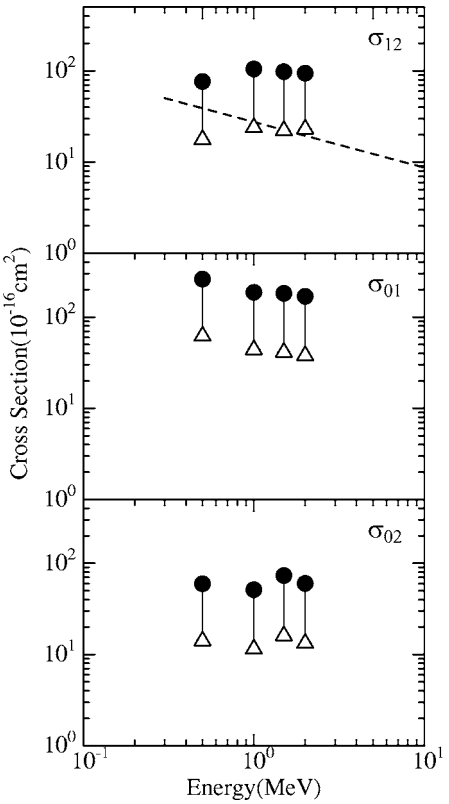

FIG. 7. Electron loss cross sections for helium projectiles. Symbols are the same as in Fig. 6. The dashed line represents loss cross sections calculated from Eq. (10).

by dot-dashed lines. The experimental cross sections seem to be reproduced fairy well by including these K-K transfer cross sections above 1 MeV.

It is interesting to compare our single-capture cross sections with the COB model which is known to give reasonable values at low impact velocities [5–8]. For a collision between a low-q ion and C_{60}, Larsson *et al.* [5] introduced a formula

$$\sigma = \frac{\pi}{2}[(1+2\sqrt{q})I_0^{-1} + r_0]^2, \tag{15}$$

where $r_0=6.7$ is the C_{60} molecular radius and $I_0=0.28$ (7.6 eV) is the ionization potential of C_{60}. This formula differs from [5] by a factor of 1/2 which we used as the transition probability of the electron from C_{60} to the incident ion at the maximum barrier height. Capture cross sections are obtained as 13×10^{-15} cm^2 for $q=1$ and 18×10^{-15} cm^2 for $q=2$ and are plotted as dashed arrows in the figure. Our cross sections seem to approach the COB values reasonably.

Electron loss cross sections for helium projectiles are shown in Fig. 7. Cross sections are nearly flat without revealing any significant energy dependence, whereas Bohr's formula of Eq. (10) (dashed line) predicts v_p^{-1} dependence. Bohr's cross sections are, however, again within a range of our experimental data.

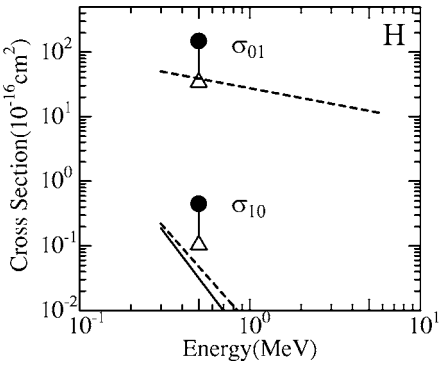

FIG. 8. Electron capture and loss cross sections for hydrogen projectiles measured at 0.5 MeV. Calculated values from Eqs. (9) and (10) are shown by dashed lines and a solid line from Eq. (14).

Finally, capture and loss cross sections obtained for hydrogen projectiles are shown in Fig. 8 together with Bohr's cross sections.

In summary electron capture and loss cross sections have been measured for fast helium and hydrogen projectiles in collisions with a gas-phase C_{60} target. We present here two sets of absolute cross sections obtained by using two different vapor pressure data. Namely, one is taken from [11] which is actually the first experimental work about the C_{60} vapor pressure and is recognized as the most reliable data. The other one is taken from [14] which is the latest experimental work and differs from the former values by a factor of 3–5 in the temperature range investigated here. At the present stage it may be fair to use both data because we cannot judge which one is better. Experimental cross sections were examined by comparing them with theoretical calculations made by using well-known formulas available in the literature. Our cross sections are found to be reasonably in agreement with these theoretical values at both low and high impact energies. Interesting results are the equilibrium charge fractions $f_q(\infty)$, obtained from the complete set of our experimental cross sections. We found that there exists essentially no gas-solid difference between a gas-phase C_{60} and a carbon foil. This result may be attributed to our low z_1 projectiles because the predominant electronic shell relevant to charge-changing collisions may be limited to the $1s$ shell only. Thus, it is interesting to extend this to high-z_1 projectiles since such multiple-electron projectiles, containing rather complicated shell structures, may certainly provide more detailed insight into the gas-solid difference involving fullerene particles.

ACKNOWLEDGMENT

This work was supported by a Grant-in-Aid for Scientific Research (B), No. 16360474, from the Japan Society for the Promotion of Science.

[1] H. W. Kroto, J. R. Heath, S. C. O'Brien, R. F. Curl, and R. E. Smalley, Nature (London) **318**, 162 (1985).
[2] E. E. B. Campbell and F. Rohmund, Rep. Prog. Phys. **63**, 1061 (2000).
[3] B. Walch, C. L. Cocke, R. Voelpel, and E. Salzborn, Phys. Rev. Lett. **72**, 1439 (1994).
[4] N. Selberg *et al.*, Phys. Rev. A **53**, 874 (1996).
[5] M. O. Larsson, P. Hvelplund, M. C. Larsen, H. Shen, H. Cederquist, and H. T. Schmidt, Int. J. Mass. Spectrom. **177**, 51 (1998).
[6] S. H. Schwartz, A. Fardi, K. Haghighat, A. Langereis, H. T. Schmidt, and H. Cederquist, Phys. Rev. A **63**, 013201 (2000).
[7] A. Bárány and C. J. Setterlind, Nucl. Instrum. Methods Phys. Res. B **98**, 184 (1995).
[8] H. Cederquist *et al.*, Phys. Rev. A **61**, 022712 (2000).
[9] L. C. Northcliffe and R. F. Schilling, Nucl. Data, Sect. A **7**, 233 (1970).
[10] L. H. Toburen, M. Y. Nakai, and R. A. Langley, Phys. Rev. **171**, 114 (1968).
[11] J. Abrefah, D. R. Olander, M. Balooch, and W. J. Siekhaus, Appl. Phys. Lett. **60**, 1313 (1992).
[12] A. Popovic, G. Drazic, and J. Marsel, Rapid Commun. Mass Spectrom. **8**, 985 (1994).
[13] V. Piacente, G. Gigli, P. Scardala, A. Gliustini, and D. Ferro, J. Phys. Chem. **99**, 14052 (1995).
[14] R. Jaensch and W. Kamke, Mol. Mater. **13**, 163 (2000).
[15] H. D. Betz, Rev. Mod. Phys. **44**, 465 (1972).
[16] H. Tawara, T. Kato, and Y. Nakai, At. Data Nucl. Data Tables **32**, 235 (1985).
[17] R. K. Janev, R. A. Phaneuf, and H. Hunter, At. Data Nucl. Data Tables **40**, 249 (1988).
[18] K. Shima and H. Tawara, At. Data Nucl. Data Tables **51**, 173 (1992).
[19] B. Bransden and M. McDowell, *Charge Exchange and the Theory of Ion-Atom Collisions* (Clarendon Press, Oxford, 1992).
[20] E. W. McDaniel, J. B. A. Mitchell, and M. E. Rudd, *Atomic Collisions—Heavy Particle Projectiles* (John Wiley & Sons, New York, 1993).
[21] N. Bohr, K. Dan. Vidensk. Selsk. Mat. Fys. Medd. **18**, 71 (1948).
[22] N. Bohr and J. Lindhard, K. Dan. Vidensk. Selsk. Mat. Fys. Medd. **28**, 7 (1954).
[23] D. Brandt, Nucl. Instrum. Methods Phys. Res. **214**, 93 (1983).
[24] I. Ben-Itzhak, A. Jain, and O. L. Weaver, J. Phys. B **26**, 1711 (1993).
[25] M. J. Puska and R. M. Nieminen, Phys. Rev. A **47**, 1181 (1993).
[26] O. Hadjar, R. Hoekstra, R. Morgenstern, and T. Schlathölter, Phys. Rev. A **63**, 033201 (2001).
[27] L. I. Pivovar, M. T. Novikov, and V. M. Tabaev, Sov. Phys. JETP **14**, 20 (1962); **15**, 1035 (1962).
[28] P. Hvelplund and E. H. Pedersen, Phys. Rev. A **9**, 2434 (1974).
[29] A. Itoh, M. Asari, and F. Fukuzawa, J. Phys. Soc. Jpn. **48**, 943 (1980); **49**, 1513 (1980).
[30] J. C. Armstrong, J. V. Mullendore, W. R. Harris, and J. B. Marion, Proc. Phys. Soc. London **86**, 1283 (1965).
[31] H. B. Gilbody, Adv. At., Mol., Opt. Phys. **33**, 149 (1994).
[32] K. Ishii, A. Itoh, and K. Okuno, Phys. Rev. A **70**, 042716 (2004).
[33] G. Lapicki and F. D. McDaniel, Phys. Rev. A **22**, 1896 (1980).